Phase-separated magnetic ground state in $Mn_3Ga_{0.45}Sn_{0.55}C$

E. T. Dias,[1] K. R. Priolkar,[1,*] A. K. Nigam,[2] R. Singh,[3] A. Das,[3] and G. Aquilanti[4]
[1]*Department of Physics, Goa University, Taleigao Plateau, Goa 403206, India*
[2]*Tata Institute of Fundamental Research, Dr. Homi Bhabha Road, Colaba, Mumbai 400005, India*
[3]*Solid State Physics Division, Bhabha Atomic Research Centre, Trombay, Mumbai 400085, India*
[4]*Elettra-Sincrotrone Trieste S.C.p.A., Strada Statale 14, km 163.5, I-34149 Basovizza, Trieste, Italy*
(Received 18 August 2016; revised manuscript received 19 January 2017; published 14 April 2017)

The existence of nonergodic ground states is considered as a precursor to a first-order long-range magnetostructural transformation. $Mn_3Ga_{0.45}Sn_{0.55}C$ lies compositionally between two compounds, Mn_3GaC and Mn_3SnC, undergoing first-order magnetic transformation. However, $Mn_3Ga_{0.45}Sn_{0.55}C$, which crystallizes in a single-phase cubic structure, exhibits more than one long-range magnetic transition. Using a combination of magnetization, ac susceptibility, neutron diffraction, and x-ray-absorption fine-structure techniques, it is shown that, although $Mn_3Ga_{0.45}Sn_{0.55}C$ exhibits long-range magnetic order, it presents a cluster glassy ground state due to formation of magnetically ordered Ga-rich and Sn-rich clusters. The clusters are big enough to present signatures of long-range magnetic order but are distributed in a way that limits interactions between two clusters of the same type, leading to a frozen magnetic state at low temperatures. The main reason for such a cluster-glass state is the difference in the local structure of Mn atoms that find themselves in Ga-rich and Sn-rich clusters.

DOI: 10.1103/PhysRevB.95.144418

I. INTRODUCTION

In favoring a ground state with minimum possible energy at absolute zero the third law of thermodynamics brings about a wide range of disorder to order transitions in systems [1]. Structural and functional materials exhibiting ordering of physical quantities such as magnetic moment, electric dipole, and lattice strain [2] satisfy thermodynamic requirements, while systems with quenched disorder or frozen randomness undergo nonthermodynamic transitions that bring about novel behaviors [3]. The widely encountered "glassy" state is known to rely on the slowing down of kinetics [4–6], which challenges the fundamental "hypothesis of ergodicity" [5,7]. Within the area of magnetic alloys, spin glasses and cluster spin glasses exemplify the existence of a glassy state in ferromagnetic systems. For instance, even a normal ferromagnet like iron when diluted by nonferromagnetic impurities (e.g., AuFe alloys) undergoes a transformation to a glassy state due to competition between ferromagnetic and antiferromagnetic interactions [8]. Similar literature reports on dielectric properties of $BaTiO_3$ reveal a change from the classical paraelectric to ferroelectric phase transition towards a diffused ferroelectric or relaxor kind as the concentration of the point defects (e.g., La^{3+}) is increased [9–11]. Governed by the same physical principle of destruction of long-range order due to strong frozen disorder, a different class of glass referred to as "strain glass" (or glassy-R martensite) can be obtained by doping point defects into a normal martensitic alloy. Doping excess nickel ($\sim$1.5%) into the widely recognized martensitic NiTi alloy destroys the martensitic transformation by creating a strain-glass regime, giving rise to a nonmartensitic ($Ti_{48.5}Ni_{51.5}$) alloy that continues to exhibit properties like the shape memory effect and superelasticity that otherwise stringently depend on the reversible martensitic transformation [12–14].

Founded in frustration and randomness of isolated moments, a study of the functional properties of disordered alloys [15–20] grew in the hope of understanding their formation, magnetic ordering, and the long-range Ruderman-Kittel-Kasuya-Yoshida (RKKY) interactions between them [8]. Among the existing geometrically frustrated $3d$ transition-metal-based antiperovskite compounds displaying a fascinating array of properties ranging from giant magnetoresistance [21,22] to a large magnetocaloric effect (MCE) [23–25], two isostructural compounds, Mn_3GaC and Mn_3SnC, exhibiting first-order, volume-discontinuous magnetostructural transitions have been extensively studied. Technologically significant properties such as a large inverse table like MCE in Mn_3GaC have been attributed to the first-order transition ($T \simeq 160$ K) from a ferromagnetic (FM) to an antiferromagnetic (AFM) state described by the propagation vector $k = [\frac{1}{2}, \frac{1}{2}, \frac{1}{2}]$ [24,26]. Although, theoretically, the magnetic properties of such antiperovskite compounds originate from strongly hybridized Mn $3d$ and C $2p$ states [27–30], ample differences have been identified in the magnetic properties exhibited by Mn_3SnC. Replacing Sn at the Ga site not only causes the first-order transition to be expressed at the paramagnetic (PM) to ferrimagnetic ordering at much higher temperatures ($\sim$280 K) but also causes the MCE to change to the conventional type with little or no field variation seen in the position of the magnetic entropy peak [31–33]. Our previous work describing the effect of Sn substitution on magnetic properties of $Mn_3Ga_{1-x}Sn_xC$ compounds illustrates the evolution of this first-order transition while highlighting the coexistence of magnetic phases for $0.41 \leqslant x \leqslant 0.71$ [32]. Questions arise as to how the two magnetic phases are supported in one crystal structure with magnetic atoms occupying equivalent lattice sites. Do the two magnetic phases interact with each other, and if they do, what could be the most physically accepted ground state of these compounds?

Generally, frustrations in a system leading to nonergodic ground states occur when impurities are added to a compound undergoing a phase transformation as in the

*krp@unigoa.ac.in

case of AuFe alloys or La-doped $BaTiO_3$ or Ni-rich NiTi alloys. $Mn_3Ga_{0.45}Sn_{0.55}C$ belongs to that region of coexisting magnetic phases in the magnetic phase diagram of $Mn_3Ga_{1-x}Sn_xC$. Although the compound crystallizes with a cubic antiperovskite-type structure (space group $Pm\bar{3}m$) that has crystallographically equivalent Mn atoms at the face centers, C at the body center, and Ga or Sn atoms occupying the corners of the cube, magnetization results showcase two apparent first-order transitions. The first magnetic transition is from an "enhanced paramagnetic" state [34] to an AFM order at 155 K akin to that in Mn_3GaC, followed by a rapid increase in magnetization to a ferromagnetic state with distinct similarities to results obtained for Mn_3SnC. Therefore the interest of this paper lies in the unprecedented significance of discovering a nonergodic ground state in a solid solution where both the end members, Mn_3GaC and Mn_3SnC, undergo a first-order transformation.

II. EXPERIMENT

The spatial distribution of coexisting phases in polycrystalline $Mn_3Ga_{0.45}Sn_{0.55}C$ has been studied using a combination of various diagnostic tools. Synthesis of the antiperovskite material used for all characterizations was done using the solid-state reaction technique wherein a stoichiometric mixture of the starting materials in elemental form (Mn, Ga, Sn, and C) along with 15 wt % excess carbon powder was mixed and pressed into a pellet that was sealed in an evacuated quartz tube. The sealed tube was initially heated at 1073 K for the first 48 h, and the final annealing was carried out at 1150 K for 120 h. Field- and temperature-dependent magnetic characterizations in the 5 to 390 K temperature range in applied magnetic fields of 0.01 and 0.5 T and between ± 7 T were carried in a Magnetic Property Measurement System (Quantum Design) using protocols described in Ref. [32]. The phase purity and structure of the prepared compound were obtained from a room-temperature x-ray diffraction pattern recorded using Cu K_α radiation. Neutron diffraction data at various temperatures were collected on the PD2 neutron powder diffractometer ($\lambda = 1.2443$ Å) at the Dhruva Reactor (Bhabha Atomic Research Center, Mumbai, India). The ac magnetic susceptibility measurements were performed using a Physical Properties Measurement System (Quantum Design). Measurements in the 2–300 K temperature range were carried out at various excitation frequencies ($33 \leqslant f \leqslant 10\,000$ Hz) by applying an ac amplitude $H_{ac} = 10$ Oe after cooling the sample in zero field [35]. The local structure surrounding the Mn_6C octahedra in the compound $Mn_3Ga_{0.45}Sn_{0.55}C$ was studied using extended x-ray absorption fine-structure (EXAFS) spectra recorded at the XAFS beamline at Elettra, Trieste [36]. Both incident (I_0) and transmitted (I) intensities were simultaneously measured at the Mn K edge (6539 eV) within the -200 to 1300 eV range using an ionization chamber filled with appropriate gases at 300 K [room temperature (RT)] and 80 K [liquid-nitrogen temperature (LT)]. An optimized value of the absorption edge jump $\Delta\mu$ in transmission mode was obtained by selectively adjusting the number of piled layers of $Mn_3Ga_{0.45}Sn_{0.55}C$ powder-coated scotch tape. Prior to reducing the Mn K-edge data to obtain the EXAFS [$\chi(k)$] signal using well-established procedures in the Demeter program [37], the edge energy was calibrated to be in tune with the first inflection point of Mn metal foil.

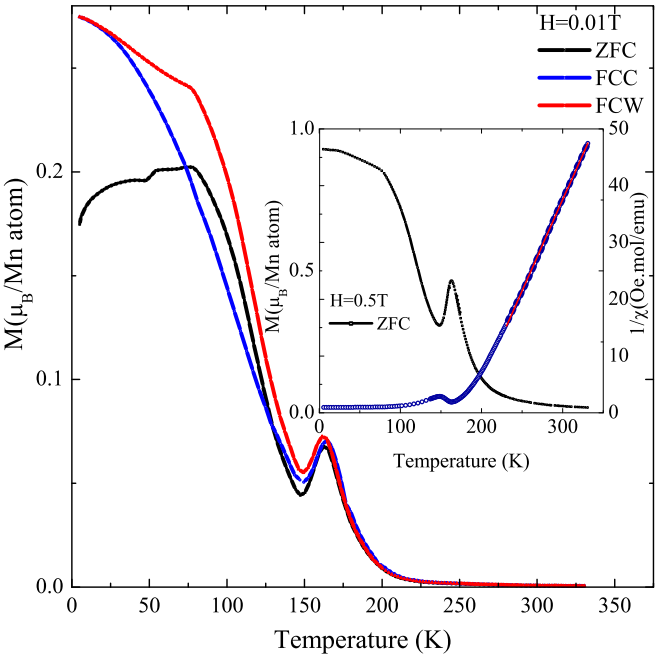

FIG. 1. Magnetic characterization of $Mn_3Ga_{0.45}Sn_{0.55}C$ between 5 and 300 K in an applied field of 0.01 T under zero-field-cooled (ZFC), field-cooled cooling (FCC), and field-cooled warming (FCW) processes. The inset shows the inverse susceptibility plot of the ZFC data at $H = 0.5$ T.

III. RESULTS AND DISCUSSION

The Rietveld refined x-ray diffraction pattern confirms the formation of a single antiperovskite phase with minor impurities of C and MnO (each less than 0.5%). However, magnetization results highlight the coexistence of competing magnetic phases. Recorded in the 5–300 K temperature range with an applied field of 0.01 T, the magnetization curve in Fig. 1 exhibits a transition from an "enhanced paramagnetic" state to an AFM state at $\sim$155 K followed by a rapid increase in magnetization arising due to ferromagnetic interactions characteristic of Sn-rich regions [32].

The marked hysteresis observed between the cooling and warming curves establishes the first-order nature of both these transitions. Apart from the large splitting observed between zero-field-cooled (ZFC) and field-cooled (FC) curves a broad maximum is seen in the ZFC curve in the ferromagnetic state ($\sim$30 K), below which the magnetization decreases with decreasing temperature. A Curie Weiss fit, as shown in the inset of Fig. 1, to high-temperature magnetization data recorded at 0.5 T gives a PM Curie temperature $\theta_P = 182$ K. Based on this quite large and positive value of θ_P, the observed decrease in magnetization in the ZFC curve cannot be interpreted as a transition to the AFM state [38].

To further explore the complexity of the magnetostructural ordering in this compound, neutron diffraction patterns recorded between 6 and 300 K in the angular range of 3°–135° were analyzed. Using the Rietveld method implemented in

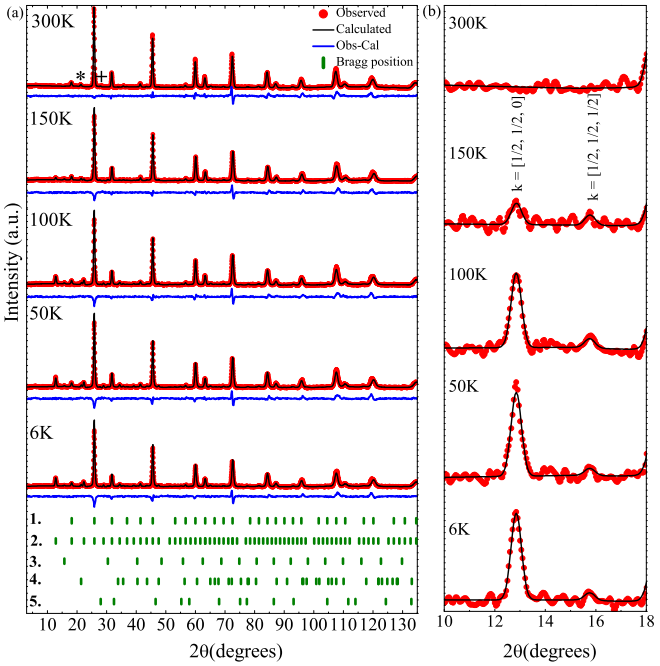

FIG. 2. (a) Series of Rietveld refined neutron diffraction patterns between 6 and 300 K. Enumerated Bragg positions correspond to (1) $Mn_3Ga_{0.45}Sn_{0.55}C$ (chemical unit cell), magnetic reflections of $Mn_3Ga_{0.45}Sn_{0.55}C$ associated with propagation vectors (2) $k = [\frac{1}{2},\frac{1}{2},0]$ and (3) $k = [\frac{1}{2},\frac{1}{2},\frac{1}{2}]$, (4) graphite (an asterisk indicates the most intense peak at 300 K), and (5) MnO (the maximum peak is indicated by a plus sign at 300 K). (b) Angular 2θ range between 10° and 18° highlighting the temperature-dependent development of magnetic peaks associated with the long-range AFM order in $Mn_3Ga_{0.45}Sn_{0.55}C$.

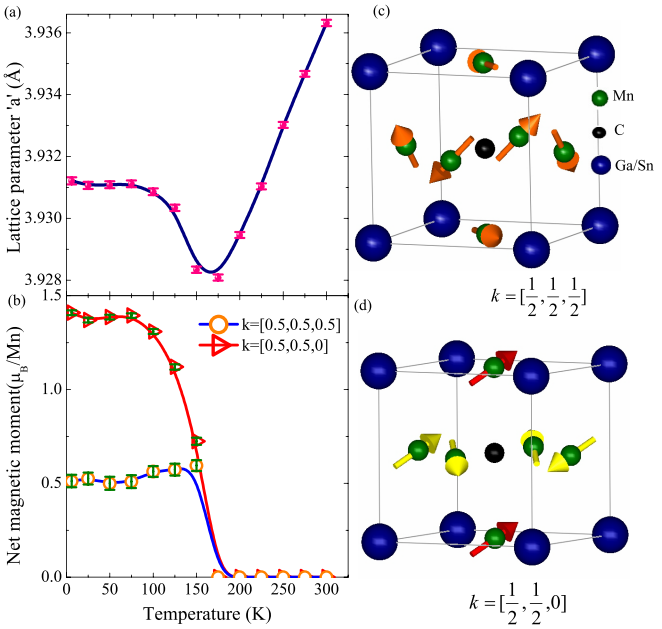

FIG. 3. (a) $Mn_3Ga_{0.45}Sn_{0.55}C$ lattice parameter variation between 6 and 300 K. (b) Thermal evolution of the averaged ordered AFM components. (c) and (d) Three-dimensional representations of the magnetic spins associated with the $Mn_3Ga_{0.45}Sn_{0.55}C$ structure as determined from the neutron diffraction pattern recorded at 6 K.

the FULLPROF suite of programs [37], the crystal structure in the PM state was refined from diffraction data collected at 300 K. Refinement results presented in Fig. 2(a) are consistent with the Rietveld refined room-temperature x-ray diffraction pattern in Ref. [32]. Occupancy parameters of Mn, Ga, Sn, and C atoms obtained through iterative refinements of neutron and x-ray diffraction patterns [39] (Mn $= 2.95 \pm 0.03$, Ga $= 0.49 \pm 0.04$, Sn $= 0.51 \pm 0.04$, and C $= 1.01 \pm 0.01$) are well within the error range. In particular, the occupancy parameters of C and Mn were obtained from refinement of neutron diffraction patterns, while those of Ga and Sn were obtained from refinement of x-ray diffraction patterns. The crystal structure is cubic at all temperatures, but the thermal evolution of lattice parameters plotted in Fig. 3(a) shows a discontinuity at about 155 K which coincides with enhanced paramagnetic to AFM transition. At 300 K, the lattice constant $a = 3.93632(9)$ Å obtained for $Mn_3Ga_{0.45}Sn_{0.55}C$ lies between that of Mn_3GaC and Mn_3SnC [32]. With decreasing temperature the lattice parameter decreases almost linearly down to 175 K before undergoing an abrupt increase of about 0.3% at $T \simeq 150$ K. Beyond this the unit cell parameter remains almost constant down to 6 K.

A closer look at Fig. 2 points to the fact that as temperature decreases, additional reflections that cannot be described solely on the basis of the chemical unit cell begin to appear for $T \leqslant 150$ K. Contemplating the magnetization results and the temperatures at which these new peaks begin to appear, one can assume them to be of magnetic origin. A search for a wave vector that yields intensities corresponding to this set of magnetic reflections indicated that the extra peaks could only be indexed assuming two magnetic propagation vectors, $k = [\frac{1}{2},\frac{1}{2},\frac{1}{2}]$ and $k = [\frac{1}{2},\frac{1}{2},0]$, that order independently of each other. Figure 2(b), featuring a magnified view of the 10°–18° 2θ range, highlights the magnetic peaks associated with these two vectors.

Fixing the magnetic reflections to an absolute scale determined by nuclear reflections in the chemical unit cell at 300 K, the thermal evolution of magnetic moments was studied in detail. The arrows in Figs. 3(c) and 3(d) provide a graphic illustration of the magnetic coupling observed between ordered Mn moments in the cubic unit cell of the compound $Mn_3Ga_{0.45}Sn_{0.55}C$ at 6 K. As portrayed in Fig. 3(c), Mn spins in the (111) planes have collinear alignment; however, two such consecutive (111) planes couple antiferromagnetically, giving rise to a doubled unit cell associated with the $[\frac{1}{2},\frac{1}{2},\frac{1}{2}]$ propagation vector. The magnetic moment per Mn atom was determined to be $0.59\mu_B \pm 0.03\mu_B$, compared to $1.54\mu_B$ obtained for Mn_3GaC at 150 K [40]. The stronger magnetic reflection at $2\theta = 12.8^\circ$ indexed using the $[\frac{1}{2},\frac{1}{2},0]$ wave vector generates the spin alignment exemplified in Fig. 3(d). The unit-cell parameters for the resulting magnetic model are $a\sqrt{2}$, $a\sqrt{2}$, and a, where a is the lattice parameter of the chemical unit cell. Although the Mn spins confined to the a–b plane are coupled antiferromagnetically, a small canting along the $[\frac{1}{2},\frac{1}{2},0]$ direction gives rise to a net ferromagnetic moment $(0.37\mu_B \pm 0.2\mu_B)$ and is responsible for the rapid rise of magnetization below 150 K. The temperature variation of the magnetic moment plotted in Fig. 3(b) indicates that both

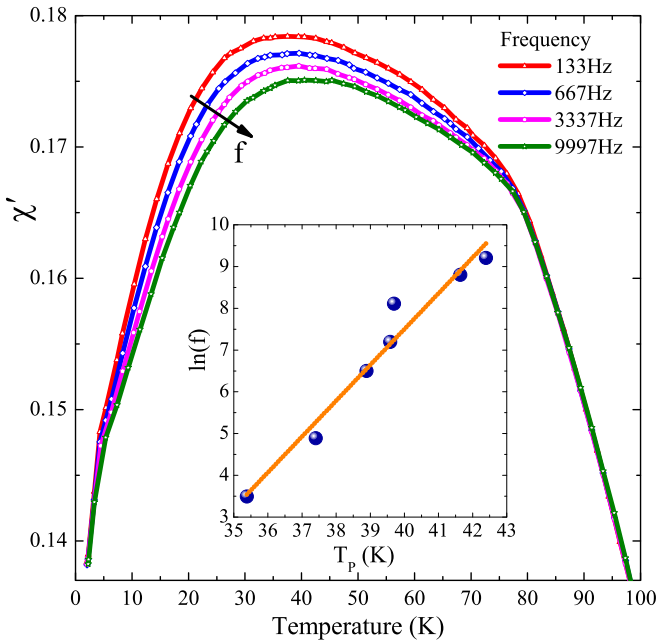

FIG. 4. Temperature dependence of the real part of the ac susceptibility measured for $Mn_3Ga_{0.45}Sn_{0.55}C$ between 2 and 100 K at different frequencies. The inset shows the variation of the peak temperature T_P with the frequency of the ac field in a Vogel-Fulcher plot.

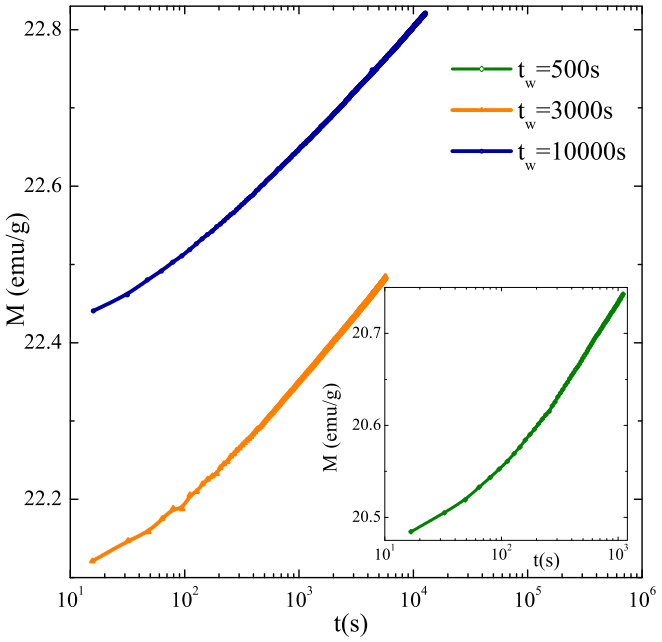

FIG. 5. Magnetization M as a function of time t at 10 K recorded under a magnetic field of 0.01 T after the sample was cooled in the ZFC mode followed by a subsequent waiting time of $t_w = 500$, 3000, and 10 000 s.

magnetic phases have the same ordering temperature of about 150 K, which coincides with the volume expansion of the chemical unit cell [Fig. 3(a)].

Overwhelming experimental evidence of the existence of two magnetically ordered phases, both antiferromagnetic but one with a finite net magnetic moment over a substantial temperature regime, naturally spurs interest in the phase-separated nature of the compound. The questions are whether the two magnetic phases interact and, if so, if this interaction results in any kind of frozen order. The understanding of magnetic interaction between the two magnetic phases is important due to differences in behavior of ZFC and FC magnetization at low temperatures. Characteristic signatures of a glassy behavior include (a) deviation of the ZFC curve from the FC curves [41], (b) the frequency dependence of low-field ac susceptibility, (c) the presence of disordered structure, and (d) local or short-range order [2]. In the present case, despite the fact that the broad maximum observed in the ZFC curve in Fig. 1 is typical for both spin-glass and cluster-glass materials, the continuous increase in magnetization with decreasing temperature as observed in the field-cooled curves of $Mn_3Ga_{0.45}Sn_{0.55}C$ suggests cluster glass is more probable than a spin-glass state.

To further confirm the glassy nature of the ground state of this compound, the ac susceptibility was measured at frequencies varying between 33 and 9997 Hz across the entire temperature range, with an ac driving field of 10 Oe. The temperature dependence of the real (χ') component of the ac susceptibility displayed in the main panel of Fig. 4 summarizes the results of the ac magnetic susceptibility between 2 and 100 K. The observed maximum T_f with a clear frequency dependence, i.e., a systematic shift towards higher temperatures with decreasing amplitudes observed for increasing frequencies, is characteristic of magnetic glassy transitions. A logarithmic frequency dependence of the peak temperature defined as a maximum on the χ' curve follows the Vogel-Fulcher empirical law fairly well, as shown in the inset of Fig. 4, which is indicative of a *glassy* ground state with frozen magnetic moments. The relative shift of spin freezing temperature ($\delta T_f = \triangle T_f / T_f \triangle \ln \nu$, where $\triangle$ represents a change in the corresponding quantity), estimated as 0.0797, lies between the values reported for canonical spin glasses ($\delta T_f = 0.0045$ for AuMn) [42] and superparamagnetic systems [$\delta T_f = 0.28$ for α–$Ho_2O_2(B_2O_3)$] [7] and is close to that of typical cluster glass systems [43].

These results imply that the compound undergoes one or more relaxation processes with characteristic relaxation time constants. A study of the time-dependent response of magnetic spins in ZFC magnetization was carried out using the following protocol. The sample was first cooled from 300 K to the measurement temperature ~10 K in zero applied field. A waiting time t_w was used to equilibrate the spin system before applying a magnetic field of 0.01 T and recording magnetization M as a function of observation time t [17,35,44]. The time-dependent response of the magnetic spins in the present compound to the external applied field is characterized by a distribution of two or more relaxation times as indicated by the exponential growth of M versus t variation in Fig. 5.

Neutron diffraction studies indicate the presence of two long-range antiferromagnetic orders coexisting below 150 K. These two antiferromagnetic orders are similar to those in the two end members, Mn_3GaC and Mn_3SnC, therefore pointing towards a magnetic phase separation into Ga-rich and Sn-rich regions. Formation of such clusters is also supported by ac susceptibility studies wherein the peak in χ' follows the

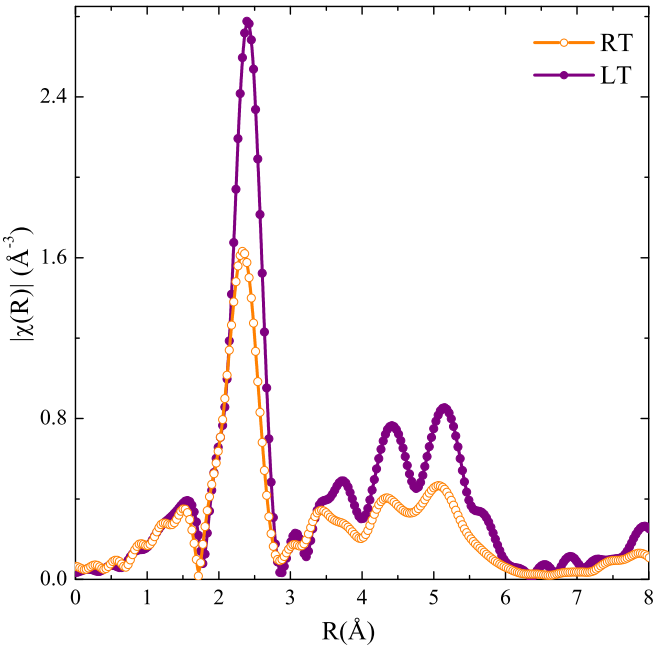

FIG. 6. Magnitude of Fourier transformed EXAFS spectra obtained at the Mn K edge in $Mn_3Ga_{0.45}Sn_{0.55}C$ at room temperature (RT) and liquid-nitrogen temperature (LT).

Vogel-Fulcher law as a function of frequency. However, structurally, the compound crystallizes in a single phase. This is despite the fact that the unit cell of Mn_3SnC is larger (∼3%) than that of Mn_3GaC. This points towards the presence of local structural distortions, especially around Mn atoms.

To probe for such possible distortions in the local structure of the Mn that could explain the coexistence of two magnetic phases EXAFS data recorded at the Mn K edge in $Mn_3Ga_{0.45}Sn_{0.55}C$ at RT and LT were analyzed. Magnitudes of the Fourier transform (FT) of both sets of EXAFS data $\chi(k)$, extracted over a k range of 3.0–14.0 $Å^{-1}$, exhibit two peaks in the R range of 0 to 3 Å, as shown in Fig. 6. The first peak results from scattering by the two nearest-neighbor C atoms, while the second and the main peak around 2.5 Å includes contributions from the next-nearest neighbors, i.e., Mn, Ga, and Sn atoms. The presence of local structural distortions can also be seen from the RT and LT plots in Fig. 6. With a decrease in temperature, all peaks grow in intensity due to the decrease in mean-square disorder in atomic positions, but the peak due to Mn-C correlation exhibits only a small increase. This is a clear indication of the presence of local structural disorder.

EXAFS spectra were fitted to two different structural models. The first one was based on the cubic structure of the compounds (referred to as Cubic model), and all the bond distances were allowed to contract or expand by the same factor. The resulting best-fit calculation in R space shows reasonably good agreement with the experimental data. In particular, we found that the bonds are contracted by 1% with respect to the starting structural cubic model (see Table I).

In order to get better agreement by accounting for atomic size differences between Mn, Ga, and Sn, in the second model the structural restrictions were relaxed, and the individual correlations were allowed to vary independently (referred to as DelR model). Although, as in the previous case, the fit was reasonably good, the obtained Mn-Sn bond distance was shorter than the Mn-Ga bond distance (see Table I). This is impossible because as the Sn atom is larger than the Ga atom, the Mn-Sn bond distance would be longer than Mn-Ga distance. Furthermore, this model also resulted in very low values of σ^2, especially for the Mn-Ga and Mn-C-Mn-C focused multiple-scattering path at 3.91 Å. Due to the increase in the number of free parameters, the statistical error bars obtained from fitting were also quite large. Thus, despite a very low R factor, this model is less reliable.

The above analysis indicates that it would be difficult to map the local disorder without any prior knowledge of at least one or two of the Mn-Ga, Mn-Mn, and Mn-Sn bond distances. To get a sense of the local structure around Mn we tried a different approach of using a linear combination fitting (LCF) with the experimental spectra of Mn_3GaC and Mn_3SnC at respective temperatures as standard components to describe the EXAFS spectra of $Mn_3Ga_{0.45}Sn_{0.55}C$ at RT and LT. This was done using the LCF routine of the ATHENA software package [37]. Constraints such as reference spectra having no negative components and the sum of coefficients normalizing to unity were imposed while fitting the data in k space in the range 3.0–14.0 $Å^{-1}$ with k weights of 1, 2, and 3. The k^2-weighted Mn K-edge EXAFS data along with the

TABLE I. Local structural parameters obtained from Mn K-edge EXAFS analysis recorded at room temperature in $Mn_3Ga_{0.45}Sn_{0.55}C$. Here C.N. is the coordination number, R_{300K} is the bond distance calculated from neutron diffraction data recorded at 300 K, R denotes the bond distances obtained from EXAFS analysis, and σ^2 denotes the mean-square disorder in R obtained from EXAFS analysis.

			Cubic model		DelR model	
Bond	C.N.	R_{300K} (Å)	R (Å)	σ^2	R (Å)	σ^2
Mn-C	2	1.968	1.948(2)	0.002(1)	1.953(12)	0.004(1)
Mn-Mn	8	2.783	2.755(2)	0.009(1)	2.748(27)	0.006(1)
Mn-Ga	4	2.783	2.755(2)	0.003(2)	2.827(48)	0.00001(900)
Mn-Sn		2.783	2.755(2)	0.005(3)	2.806(43)	0.001(10)
Mn-C-Mn	16	3.359	3.326(2)	0.02(5)	3.146(68)	0.003(10)
Mn-Mn_2	6	3.936	3.896(2)	0.014(4)	3.829(37)	0.009(3)
Mn-C-Mn_2	4	3.936	3.896(2)	0.009(3)	3.868(30)	0.002(2)
Mn-C-Mn_2-C	2	3.936	3.896(2)	0.004(2)	3.907(24)	0.0006(10)
R factor			0.0359		0.0057	

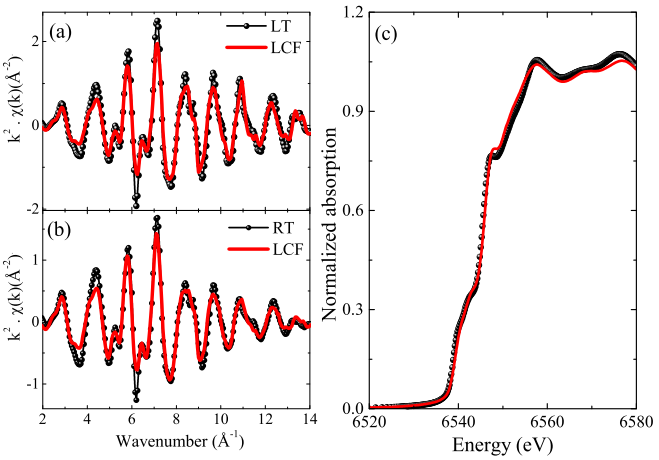

FIG. 7. The k^2-weighted EXAFS spectra of $Mn_3Ga_{0.45}Sn_{0.55}C$ recorded at (a) the low-temperature Mn K edge and (b) the room-temperature Mn K edge and the corresponding linear combination fit (solid line). (c) LCF analysis of the XANES region (−20 to +30 eV with respect to the absorption edge) of the Mn K edge in $Mn_3Ga_{0.45}Sn_{0.55}C$.

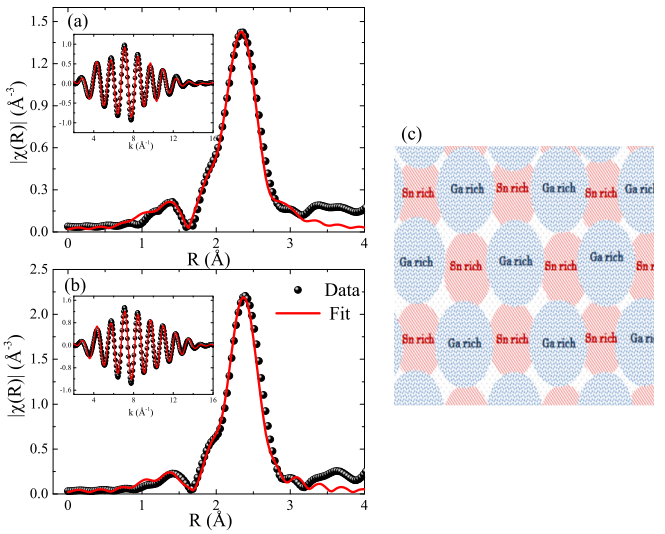

FIG. 8. The magnitude of Fourier transform of k^2-weighted Mn K EXAFS spectra of $Mn_3Ga_{0.45}Sn_{0.55}C$ recorded at (a) the low-temperature Mn K edge and (b) the room-temperature Mn K edge along with corresponding best fits (solid lines). The inset shows the corresponding back-transformed spectra of the experimental data (solid spheres) and fit (solid line) in k space. (c) Pictorial representation of the magnetic glassy state formed as a result of Ga-rich and Sn-rich regions in $Mn_3Ga_{0.45}Sn_{0.55}C$.

linear combination fit at both RT and LT are given in Fig. 7. The compositions obtained were about 60% ± 3% of Mn_3GaC and 40% ± 3% of Mn_3SnC. This hinted at the possibility of Mn atoms having two different local structures. Those Mn atoms that find themselves in Ga-rich environment could have a local structure similar to that in Mn_3GaC. while those with a Sn-rich environment around them may find themselves in a local structural environment similar to Mn_3SnC. LCF analysis of the x-ray absorption near-edge structure (XANES) region (−20 to +30 eV with respect to the edge energy) using ΔE_0 values obtained in the EXAFS analysis also gave similar fractional compositions at 53% ± 4% of Mn_3GaC and 47% ± 4% of Mn_3SnC at LT and is presented in Fig. 7(c).

In order to obtain a more quantitative picture of the local structure around Mn in $Mn_3Ga_{0.45}Sn_{0.55}C$, the room temperature Mn K EXAFS data were fitted with correlations used for fitting EXAFS data of Mn_3GaC and Mn_3SnC in an R range of 1 to 3 Å and a k range of 3 to 14 Å^{-1}. It must be mentioned that at room temperature, the local structure around Mn in Mn_3GaC is as expected from the cubic symmetry [45], while the Mn_6C octahedra are distorted in Mn_3SnC [46]. Constructing a model based on the relative fractions of the correlations in Mn_3GaC and Mn_3SnC as described earlier in Refs. [45,46], respectively, and using the values of bond distances and σ^2 of various correlations obtained from fitting the EXAFS data of the two end members as first guess parameters resulted in a quite good fit, as depicted in Fig. 8(a). The relative fractions obtained were 0.52 ± 0.08 for Mn_3GaC and 0.48 ± 0.08 for Mn_3SnC.

At 100 K (LT), the local cubic symmetry around Mn is broken, and Mn-Mn and Mn-Ga bond distances are not equal [45]. Hence additional fitting parameters were introduced, setting the number of fitting parameters to 13 as opposed to 14 degrees of freedom. The number of fitting parameters were reduced to 11 by using the same σ^2 for all Mn-C paths and the same value for all Mn-Mn paths. Such a fitting also resulted in a satisfactory fit [see Fig. 8(b)], with relative fractions for Mn_3GaC and Mn_3SnC of 0.50 ± 0.08 and 0.50 ± 0.08, respectively. The parameters obtained from fitting RT and LT data are summarized in Table II.

Thus the above results clearly indicate that although $Mn_3Ga_{0.45}Sn_{0.55}C$ crystallizes in a structurally single phase, it consists of clusters that are either rich in Ga or rich in Sn distributed in a 54:46 ratio. The Mn atoms in the Ga-rich clusters order antiferromagnetically with a propagation vector along the $[\frac{1}{2},\frac{1}{2},\frac{1}{2}]$ direction as in the case of Mn_3GaC, and those

TABLE II. Bond distance R and mean-square disorder σ^2 obtained from Mn K-edge EXAFS analysis in $Mn_3Ga_{0.45}Sn_{0.55}C$ recorded at 300 K (RT) and 100 K (LT). C.N. denotes the coordination number.

		RT		LT	
Bond	C.N.	R (Å)	σ^2	R (Å)	σ^2
		Correlations of Mn_3GaC			
Mn-C	2	1.90(1)	0.005(1)	1.94(3)	0.003(1)
Mn-Mn	8	2.70(1)	0.007(1)	2.69(1)	0.005(1)
Mn-Ga	4	2.70(1)	0.003(2)	2.71(1)	0.002(1)
		Correlations of Mn_3SnC			
Mn-C	2	1.91(1) 2.07(1)	0.005(1)	1.94(1) 2.05(1)	0.003(1)
Mn-Mn	8	2.71(1) 2.93(1)	0.007(1)	2.74(1) 2.90(1)	0.005(1)
Mn-Sn	4	2.93(1) 2.71(1)	0.004(1)	2.90(1) 2.74(1)	0.005(1)

Mn atoms in the Sn-rich clusters order antiferromagnetically with a propagation vector along the $[\frac{1}{2},\frac{1}{2},0]$ direction along with a net ferromagnetic moment. These clusters are large enough to present a magnetic Bragg peak in neutron diffraction, but the interaction between two such clusters of the same type is severely limited by a cluster of the other type, causing a slowing down of kinetics and resulting in a magnetically glassy state. This clustered ground state is depicted pictorially in Fig. 8(c).

IV. CONCLUSION

In conclusion, $Mn_3Ga_{0.45}Sn_{0.55}C$, although it exhibits long-range structural ordering, presents a nonergodic ground state due to the formation of Ga-rich and Sn-rich antiferromagnetically ordered clusters with different propagation vectors. The two types of clusters are distributed in such a way that the magnetic interaction between two clusters of the same type is severely limited, thus leading to a cluster glassy ground state. The main reason for such a cluster-glass state is the difference in local structures of Mn atoms that find themselves in either a Ga-rich or Sn-rich environment.

ACKNOWLEDGMENTS

The research was supported by the Board of Research in Nuclear Sciences (BRNS), Department of Atomic Energy, Mumbai under Project No. 2011/37P/06. Experimental assistance from D. Buddhikot and G. Jangam is gratefully acknowledged.

[1] G. Careri, *Order and Disorder in Matter* (Addison Wesley, Boston, 1984).
[2] X. Ren, Y. Wang, Y. Zhou, Z. Zhang, D. Wang, G. Fan, K. Otsuka, T. Suzuki, Y. Ji, J. Zhang, Y. Tian, S. Hou, and X. Ding, Philos. Mag. **90**, 141 (2010).
[3] D. Sornette, *Critical Phenomena in Natural Sciences: Chaos, Fractals, Self Organization and Disorder: Concepts and Tools*, Springer Series in Synergetics (Springer, Berlin, 2006).
[4] B. Jerome and J. Commandeur, Nature (London) **386**, 589 (1997).
[5] K. Binder and A. P. Young, Rev. Mod. Phys. **58**, 801 (1986).
[6] L. Santen and W. Krauth, Nature (London) **405**, 550 (2000).
[7] J. A. Mydosh, *Spin Glasses: An Experimental Introduction* (Taylor and Francis, London, 1993).
[8] V. Cannella and J. A. Mydosh, Phys. Rev. B **6**, 4220 (1972).
[9] W. J. Merz, Phys. Rev. **91**, 513 (1953).
[10] R. Zhang, J. F. Li, and D. Viehland, J. Am. Ceram. Soc. **87**, 864 (2004).
[11] M. V. Petrovi, J. Bobi, T. Ramoka, J. Banys, and B. Stojanovi, Mater. Charact. **62**, 1000 (2011).
[12] S. Sarkar, X. Ren, and K. Otsuka, Phys. Rev. Lett. **95**, 205702 (2005).
[13] Y. Wang, X. Ren, and K. Otsuka, Phys. Rev. Lett. **97**, 225703 (2006).
[14] Y. Wang, X. Ren, K. Otsuka, and A. Saxena, Phys. Rev. B **76**, 132201 (2007).
[15] O. Tegus, E. Brück, L. Zhang, Dagula, K. H. J. Buschow, and F. R. de Boer, Phys. B (Amsterdam, Neth.) **319**, 174 (2002).
[16] *Introduction to Frustrated Magnetism: Materials, Experiments, Theory*, edited by P. M. C. Lacroix and F. Mila, Springer Series in Solid-State Sciences (Springer, Berlin, 2011).
[17] D. Y. Cong, S. Roth, and Y. D. Wang, Phys. Status Solidi B **251**, 2126 (2014).
[18] J. Liu, K. Skokov, and O. Gutfleisch, Scr. Mater. **66**, 642 (2012).
[19] D. Sherrington, T. Fukuda, A. Saxena, and A. Planes, *Disorder and Strain-Induced Complexity in Functional Materials* (Springer, Berlin, 2012), pp. 177–199.
[20] O. Derzhko, J. Richter, and M. Maksymenko, Int. J. Mod. Phys. B **29**, 1530007 (2015).
[21] K. Kamishima, T. Goto, H. Nakagawa, N. Miura, M. Ohashi, N. Mori, T. Sasaki, and T. Kanomata, Phys. Rev. B **63**, 024426 (2000).
[22] Y. B. Li, W. F. Li, W. J. Feng, Y. Q. Zhang, and Z. D. Zhang, Phys. Rev. B **72**, 024411 (2005).
[23] T. Tohei, H. Wada, and T. Kanomata, J. Appl. Phys. **94**, 1800 (2003).
[24] M.-H. Yu, L. H. Lewis, and A. R. Moodenbaugh, J. Appl. Phys. **93**, 10128 (2003).
[25] A. A. Aczel, L. Li, V. O. Garlea, J.-Q. Yan, F. Weickert, M. Jaime, B. Maiorov, R. Movshovich, L. Civale, V. Keppens, and D. Mandrus, Phys. Rev. B **90**, 134403 (2014).
[26] D. Fruchart, E. Bertaut, F. Sayetat, M. N. Eddine, R. Fruchart, and J. Snateur, Solid State Commun. **8**, 91 (1970).
[27] D. F. Shao, W. J. Lu, J. C. Lin, P. Tong, H. B. Jian, and Y. P. Sun, J. Appl. Phys. **113**, 023905 (2013).
[28] D. Shao, W. Lu, P. Tong, S. Lin, J. Lin, and Y. Sun, J. Phys. Soc. Jpn. **83**, 054704 (2014).
[29] J. H. Shim, S. K. Kwon, and B. I. Min, Phys. Rev. B **66**, 020406 (2002).
[30] J. P. Jardin and J. Labbe, J. Solid State Chem. **46**, 275 (1983).
[31] B. S. Wang, P. Tong, Y. P. Sun, X. Luo, X. B. Zhu, G. Li, X. D. Zhu, S. B. Zhang, Z. R. Yang, W. H. Song, and J. M. Dai, Europhys. Lett. **85**, 47004 (2009).
[32] E. T. Dias, K. R. Priolkar, and A. K. Nigam, Mater. Res. Express **1**, 026106 (2014).
[33] E. T. Dias, K. R. Priolkar, Ö. Çakir., M. Acet, and A. K. Nigam, J. Appl. Phys. **117**, 123901 (2015).
[34] Ö. Çakir and M. Acet, J. Magn. Magn. Mater. **344**, 207 (2013).
[35] T. Scholz and R. Dronskowski, AIP Adv. **6**, 055107 (2016).
[36] A. D. Cicco, G. Aquilanti, M. Minicucci, E. Principi, N. Novello, A. Cognigni, and L. Olivi, J. Phys. Conf. Ser. **190**, 012043 (2009).
[37] B. Ravel and M. Newville, J. Synchrotron Radiat. **12**, 537 (2005).
[38] H. Maletta, W. Felsch, and J. Tholence, J. Magn. Magn. Mater. **9**, 41 (1978).
[39] T. Amos, Q. Huang, J. Lynn, T. He, and R. Cava, Solid State Commun. **121**, 73 (2002).
[40] Ö. Çakir, M. Acet, M. Farle, and A. Senyshyn, J. Appl. Phys. **115**, 043913 (2014).

[41] W. Wu, C. Israel, N. Hur, S. Park, S.-W. Cheong, and A. de Lozanne, Nat. Mater. **5**, 881 (2006).
[42] C. A. M. Mulder, A. J. van Duyneveldt, and J. A. Mydosh, Phys. Rev. B **25**, 515 (1982).
[43] T. Chakrabarty, A. V. Mahajan, and S. Kundu, J. Phys. Condens. Matter **26**, 405601 (2014).
[44] S. Chatterjee and A. K. Nigam, Phys. Rev. B **66**, 104403 (2002).
[45] K. R. Priolkar, E. T. Dias, G. Aquilanti, Ö. Çakir, M. Acet, and A. K. Nigam, J. Phys. Conf. Ser. **712**, 012117 (2016).
[46] E. T. Dias, K. R. Priolkar, A. Das, G. Aquilanti, Ö. Çakir, M. Acet, and A. K. Nigam, J. Phys. D **48**, 295001 (2015).